Unravelling the mechanisms of cyanobacterial resilience in photosynthetic living materials

Henna Mustila
University of Turku
Elia Marelli
University of Turku
Sergey Kosourov
University of Turku
Yagut Allahverdiyeva-Rinne
allahve@utu.fi
University of Turku

Research Article

Keywords: Biofilm, Cyanobacteria, Engineered living materials, Hydrogel, Proteomics, Photosynthesis

Posted Date: July 27th, 2026

DOI: https://doi.org/10.21203/rs.3.rs-10413490/v1

Additional Declarations: No competing interests reported.

Abstract

Background

Photosynthetic cyanobacteria entrapped in artificial solid matrices, such as alginate hydrogels, can sustain active photosynthesis and bio-production of chemicals for months, yet the cellular adaptations underlying this remarkable resilience remain poorly understood.

Results

Here, we compared the physiological and proteomic responses of the model cyanobacterium *Synechocystis* sp. PCC 6803 entrapped within thin calcium-alginate hydrogel films with those of suspension-grown cells. Immobilized cells maintained relatively stable photosystem II (PSII) photochemical efficiency over three weeks despite strongly restricted biomass accumulation. By contrast, suspension cultures exhibited a progressive decline in phycobilisome connectivity and PSII photochemical yield during prolonged cultivation. To elucidate the molecular adaptations associated with immobilization, we applied a comparative label-free proteomics, which revealed extensive and time-dependent proteome remodelling following immobilization. Proteins involved in photoprotection, alternative electron sinks and respiratory terminal oxidases progressively increased in abundance, indicating an enhanced capacity for excitation-energy dissipation and redox balancing. In parallel, ribosomal proteins, chaperones and Rubisco subunits broadly decreased in abundance, whereas the stringent-response regulator SpoT increased, suggesting a regulated downshift in growth-related metabolism and reallocation of cellular resources towards maintenance. Increased abundance of inorganic carbon uptake systems, cell-surface and pilus-associated proteins and toxin-antitoxin modules further indicated acclimation to spatial confinement, diffusion limitations, and high local cell density within the hydrogel matrix.

Conclusion

Collectively, these findings demonstrate that entrapment in thin-layer hydrogel induces a coordinated, maintenance-oriented physiological state that preserves photosynthetic activity under growth-limited conditions, consistent with a longevity phenotype. This state shares key features with natural cyanobacterial biofilms and enables photosynthetic living materials to function as robust biocatalysts for long-term bio-production.

Background

Cyanobacteria are versatile photosynthetic cell factories with growing biotechnological potential for sustainable chemicals, fuel and material production from CO_2 and light (1–3). While conventionally cultivated in suspension, cyanobacteria are increasingly incorporated into immobilized systems to

generate long-lived biocatalysts that secrete product into surrounding medium, demonstrating several advantages over suspension cultures: easier product separation, simplified handling, higher volumetric productivity, and improved process efficiency in industrial settings (4–8). Yet, despite this growing adoption, the physiological consequences of immobilization on cyanobacterial cells remain poorly understood – a gap that limits rational optimization of these systems.

In nature, cyanobacteria commonly grow as biofilms embedded in a self-produced organic matrix, often in association with diverse microbial partners (9). Such cyanobacterial mats can grow on rocks or sediments in benthic zone or in soils crusts across a wide range of habitats (10–13). These multi-layered microbial communities are held together by extracellular polymeric substances (EPS), which maintain hydration and provide physical protection (12, 14, 15). EPS is particularly rich in polysaccharides that function as carbon reservoirs (12, 16) and facilitate surface adhesion, nutrient and metal uptake, and the maintenance of extracellular DNA and enzymes (12, 13, 17).

This capacity of cyanobacteria to thrive within biofilm matrices has attracted growing interest for biotechnological applications (revied by (4)). Artificial cyanobacterial biofilms represent a class of engineered living materials (ELMs) in which environmentally responsive cells are embedded within a polymeric scaffold that provides structural support (19, 20). Recent studies emphasize the need for durable, biodegradable and cell compatible materials for ELM construction (21–24). Cyanobacteria are particularly suitable for these systems because CO_2 readily diffuses through many matrix materials and the thin biofilm layers allow efficient light penetration, avoiding the shading limitations typical of dense planktonic cultures. Furthermore, immobilization may help mitigate the genetic instability often observed in planktonic bacterial production systems, enabling prolonged metabolic activity (25).

Biocompatible scaffolds such as calcium-alginate or TEMPO-oxidised nanofibril hydrogels offer a particularly promising route to modulating cell physiology while maintaining photosynthetic activity. These matrices provide a hydrated, semi-permeable environment that supports nutrient exchange and light penetration, while simultaneously imposing physical constraints that shape cellular behaviour (26). Advances in scaffold engineering, including polysaccharide-based and bioinspired hydrogel architectures, have markedly improved mechanical stability and enabled sustained photosynthetic activity for up to four months in immobilized systems (24, 27–29). Critically, growth restricted cells within a hydrogel can redirect photosynthetically captured light energy and carbon toward end products rather than biomass accumulation. At industrial scales, immobilization can additionally reduce operational costs by minimizing biomass harvesting, simplifying medium exchange, increasing volumetric cell density as well as reducing the risk for contamination by unwanted micro-organisms (27, 30).

Immobilized bacteria experience distinct microenvironments shaped by gradients in light, nutrients and oxygen, which can reshape gene expression, protein abundance and metabolic fluxes (31–33). Proteomic studies of immobilized *Escherichia coli* show that gel-entrapped cells do not simply mirror stationary phase planktonic cells but instead adopt unique protein expression profiles (34, 35). Physical

confinement elicits similarly distinct phenotypes in other microorganisms, including reduced cell size in yeast (36) or palmelloid aggregate formation in *Chlamydomonas reinhardtii* (31, 37).

Cyanobacterial immobilization has likewise been shown to enhance cell longevity (38), with cells embedded in natural or artificial matrices remaining viable for months without any indication of formation of resting stages such as akinetes. Yet the molecular mechanisms enabling this prolonged physiological activity remain largely unresolved - a critical knowledge gap for the rational design of long-lived biocatalytic systems.

Here we investigate the physiological responses of wild-type *Synechocystis* cells immobilized in Ca^{2+}-alginate films, combining comparative proteomics with photosynthetic performance measurements relative to planktonic cultures. By integrating spectroscopic measurements, microscope and proteomic analysis, we identify the molecular and functional adaptations underpinning immobilized cyanobacterial physiology. These findings provide a mechanistic foundation for optimizing immobilization strategies and advancing the design of robust, long-lived, photosynthetically active biocatalytic platforms.

Material and methods

1.1 Growth conditions and experimental setup

A glucose-tolerant variant of *Synechocystis* sp. PCC 6803 was cultivated at 30°C in BG-11 medium buffered with 20 mM HEPES (pH 7.5) under continuous white LED illumination (50 µmol photons $m^{-2}s^{-1}$, PAR) and aeration with 3% CO_2-enriched air.

Pre-experimental cultures (400 ml) were grown for 3 days in 225 cm² cell culture flasks (Falcon) with filter cap under agitation at 140 rpm (AlgaeTron AG 130, PSI Instruments, Czechia) to obtain sufficient biomass. The cells were then harvested, adjusted to comparable total chlorophyll *a* (Chl *a*) content and used to establish two experimental systems: (i) suspension cultures, where harvested cells were resuspended in 25 ml fresh BG-11 medium, and (ii) immobilized cultures, where cells were entrapped in Ca^{2+}-alginate films and placed in 25 ml of fresh BG-11 in Nunc non-treated T75 EasyFlask with filter caps.

Cultures were maintained under white light at 50 µmol photons m^{-2} s^{-1} and supplemented with 3% CO_2. Suspension cultures were gently agitated, whereas immobilized cultures were kept static to preserve the structural integrity of the alginate films. To support long-term cultivation, the medium was periodically replenished (see Fig. 1).

1.2 Immobilization process

The harvested cells were entrapped in thin Ca^{2+}-alginate films as described previously (39) with minor modifications. Here, cell immobilization was conducted by mixing 1 g of wet cell biomass, 0.5 ml MQ water and 1 ml 4% sodium alginate (#71238, Sigma-Aldrich). The alginate matrix gelation was initiated

by applying 50 mM $CaCl_2$ solution. Alginate films were cast as thin layers (~ 200 µm thickness) to facilitate gas exchange and light penetration. The alginate films were cut into 5 × 2 cm strips and placed into cell culture flasks containing 25 ml of BG-11 medium. Prior to the measurements, the immobilized cells were released from Ca^{2+}-alginate films by 50 mM EDTA (pH 7.0) and washed with BG-11 medium.

1.3 Sample collection for the proteomics and physiological measurement

For the proteomics and physiology analyses the samples were collected at three time points, 24 h (1 d), day 14 (14 d), and day 21 (21 d). The immobilized cells were recovered by disintegrating the alginate matrices in 50 mM Na-EDTA solution (pH 7.0). Suspended and detached cells were collected by centrifugation 6000 x g for 8 min at 4°C and washed with 50 mM TES-KOH pH 8. The samples from the four independent cultures were collected and immediately frozen with liquid N_2 and stored at -80°C until used for experiments.

1.4 Absorption spectroscopy and fluorescence measurements

Room temperature absorption spectra were measured by the OLIS CLARiTY 17 UV/VIS/NIR spectrophotometer with the integrating cavity (On Line Instrument Systems, Inc.) as described previously (40).

The chlorophyll (Chl) *a* fluorescence from intact cells released from hydrogel films was recorded with a pulse amplitude-modulated spectrophotometer (Dual-PAM-100; Walz). Harvested cells were resuspended in fresh BG-11 pH 7.5 and adjusted to 10 µg Chl a ml^{-1}. Before measurements, cells were dark-adapted for 15 min. Actinic light of 50 µmol photons m^{-2} s^{-1} was then applied and saturating pulses of 5000 µmol photons m^{-2} s^{-1} (500 ms) were used to determine the effective yield of PSII, Y(II).

The low-temperature (77 K) fluorescence emission spectra of intact cells were monitored with a USB4000-FL-450 (Ocean Optics) spectrofluorometer. Samples were adjusted to same Chl *a* concentration (5 µg ml^{-1}) and then frozen directly in liquid nitrogen. Fluorescence emission spectra were recorded upon excitation with 580 nm light.

1.5 Imaging

1 cm^2 squares were cut from the hydrogel films at day 3 and day 22 of cultivation. The cutlets were embedded in 4% agarose gels to allow for thin slicing with a Vibratome (Leica VT1200S). 150 µm thick cross sections were obtained and preserved in PBS buffer. Brightfield microscope images of the cross sections were obtained with Leitz microscope. Confocal imaging of the alginate films was performed with LSM 880 (Zeiss).

1.6 Liquid chromatography-tandem mass spectrometry

For liquid chromatography-tandem mass spectrometry (LC-ESI-MS/MS) analysis, total proteins from suspension cultures and recovered immobilised films were isolated and digested as described previously in (41). The mixture of peptides was desalted via Sep-Pack C18 (Waters) columns according to manufacturer's protocol. Dried and desalted peptide samples were reconstituted in 0.1% formic acid.

Peptides from 20 *Synechocystis* sp. PCC 6803 samples were prepared for mass spectrometry analysis. Peptide concentrations were determined using a NanoDrop spectrophotometer (Thermo Fisher Scientific), and 500 ng of peptides per sample were loaded onto Evotips (Evosep). Samples were analyzed in randomized order to minimize batch effects.

LC-ESI-MS/MS analysis was performed using an Evosep One HPLC system (Odense, Denmark) coupled to a Bruker timsTOF FLEX mass spectrometer (Bremen, Germany) equipped with a CaptiveSpray nano-electrospray ionization source. Peptides were separated on a 15 cm Evosep Performance analytical column (150 µm × 15 cm, 1.5 µm C18 beads, EV1137) using a 44-minute gradient (30 samples per day method). The mobile phases consisted of 0.1% formic acid in water (solvent A) and 0.1% formic acid in 99.9% acetonitrile (solvent B).

Data were acquired using a data-independent acquisition (DIA) method with dia-PASEF scanning. The acquisition covered an m/z range of 301–1100 and utilized two ion mobility (IM) windows per scan with variable isolation widths based on precursor density. A total of 25 dia-PASEF scans were performed per sample, with an IM range of 1.3 to 0.6 V·s/cm². Accumulation and ramp times were set to 100 ms. Data acquisition was controlled using Compass 2025b software (Bruker).

1.7 Proteomics data processing and analysis

Protein identification and label-free quantification were performed using Spectronaut software (Biognosys, version 20.1.250603.62635). The DirectDIA workflow was employed for peptide and protein identification. Quantification was based on MS2-level data using the area under the curve (AUC) of fragment ions within defined integration boundaries. Label-free quantification was performed using the MaxLFQ algorithm.

Protein identification and quantification were performed using trypsin as the proteolytic enzyme, allowing up to two missed cleavages per peptide. Carbamidomethylation of cysteine residues, introduced via iodoacetamide alkylation, was set as a fixed modification, while N-terminal acetylation and methionine oxidation were included as variable modifications. The protein search was conducted against the UniProt *Synechocystis* sp. PCC 6803 database (March 2025 release), supplemented with the Universal Protein Contaminant Database (42). Both precursor and protein false discovery rate (FDR) thresholds were set at 1%, and quantification was based on MS2-level data.

The mass spectrometry data and protein identification files data have been deposited to the ProteomeXchange Consortium via the PRIDE partner repository (43) under the dataset identifier PXD081286.

For statistical analysis, Spectronaut software was used to perform pairwise comparisons between sample groups using an unpaired *t*-test at the protein level. Differential abundance results are reported as $\log_2$ fold change (Log_2FC) values. The significantly changed proteins were filtered by a *q*-value (adjusted *p*-value) of 0.05 and an absolute Log_2FC of 0.58. Venn diagrams were made with a web-based tool (https://www.interactivenn.net/) (44).

Gene ontology (GO) enrichment analysis was performed with Spectronaut software via importing GO Consortium annotation file (modified 5.3.2026) for *Synechocystis* sp. PCC 6803 from UniProt.

2 Results and Discussion

2.1 Immobilization uncouples growth arrest from photosynthetic decline

The Chl *a* content of replenished suspension cultures increased up to day 19, while the majority of the Chl *a* increase in immobilized cells occurred within the first day of cultivation (Fig. 2A-B). Based on these growth trajectories, three time points were selected for further characterization: day 1, 14, and 21. In suspension cultures, these time points corresponded to the early logarithmic growth phase (day 1), the late growth phase (day 14), and the transition to the stationary phase as the cultures approached a plateau (day 21).

Whole-cell absorption spectra normalized to OD_{750} revealed changes in pigment-associated absorbance relative to biomass. In suspension cultures, the phycobilisome-associated peak at ~ 625 nm and the Chl *a*-associated peak at ~ 680 nm decreased slightly after day 1 and more markedly after day 14 (Fig. 2C). In immobilized cultures, both peaks remained relatively stable between day 1 and 14, with a decrease becoming apparent only by day 21 (Fig. 2D). Thus, although the total Chl *a* content per flask increased during cultivation (Fig. 2A), the OD_{750}-normalized spectra, recorded using an integrative sphere, indicated a reduction in Chl *a*- and phycobilisome-associated absorbance per unit biomass. This reduction occurred progressively and was more pronounced in suspension cultures, whereas in immobilized cultures it becomes apparent mainly between days 14 and 21. At day 1, the phycobilisome-to-Chl *a* (A_{625}/A_{680}) ratio was lower in immobilized cells (1.1 ± 0.003) than in suspension cultures (1.3 ± 0.01). During subsequent cultivation, this ratio decreased in suspension cultures but remained comparatively stable in immobilized cells, thereby reducing the difference between the two cultivation modes over time.

To assess the functional coupling between the phycobilisome antenna and the photosystems, 77 K emission spectra were measured upon excitation of phycobilisome at 580 nm. In 21 days old suspension cultures, different from immobilised cells, a strong emission peak at 685 nm was observed, implying to decoupling between phycobilisomes from PSII (Fig. 2E-F) (45–47). In agreement, effective yield of PSII (*Y(II)*) was strongly reduced in suspension cultures already at day 14 (0.21 ± 0.004) compared to day 1 (0.28 ± 0.005) with further strong decrease at day 21 (0.12 ± 0.029. Figure 2H). The

first two peaks of 77K emission spectrum, at 645 nm and 665 nm, correspond to phycocyanin and allophycocyanin emission, respectively (47). In suspension cultures, the phycocyanin peak decreased slightly on days 14 and 21 relative to day 1, while allophycocyanin emission remained unchanged (Fig. 2G).

In immobilized cultures, both phycocyanin and allophycocyanin emissions were strongly reduced already by day 14, with further reduction by day 21. Different from the suspension cultures, the effective yield of PSII in immobilized cells decreased only moderately at day 14 relative to day 1, and the further decrease at day 21 was not statistically significant (Fig. 2D).

Brightfield microscopy of freshly prepared Ca^{2+}-alginate hydrogels showed that cells were evenly dispersed throughout the hydrogel matrix (Fig. 3A, Fig. S1A, Fig. S2). After 3 and 22 days of cultivation, cell distribution within the hydrogels was examined by laser-scanning confocal microscopy using Chl *a* autofluorescence as a marker for chl-containing cells (Fig. 3B–F). The strongest fluorescence signal was consistently observed near the hydrogel surface (Fig. 3B). This may partly reflect a higher cell density in the surface layer, where cells receive more light and have better gas exchange, and is consistent with the surface-associated biomass accumulation observed as outgrowth during cultivation on the full medium. Similar phenomenon has been reported for immobilized cyanobacterial production strains, where cell escape into the surface of the entrapment matrix (48, 49). However, the high density of pigmented cells near the surface may also attenuate both the excitation light and the emitted fluorescence, thereby reducing the apparent signal intensity at greater imaging depths (Fig. 3C). A similar distribution pattern was observed on day 22, with cells still present throughout the matrix (Fig. 3, Fig. S1B, Fig. S3B). The three-dimensional reconstructions similarly showed fluorescence throughout the hydrogel volume, with a pronounced decline in intensity with depth (Fig. 3C, 3F). This gradient may result from a combination of non-uniform cell distribution and optical shielding by the densely populated surface layer. A wider-field image acquired approximately 10 µm below the surface (Fig. S3A) showed some lateral heterogeneity in fluorescence intensity. This may reflect local variation in cell distribution, hydrogel thickness, or incomplete flattening of the sample on the microscope slide.

Across both time points, the cells did not appear to form large, distinct clusters, even after prolonged cultivation. This differs from previous studies in which *Synechocystis* formed colony-like clusters when immobilized in 2.1% agarose cylinders (50) or in 4% alginate beads (51). The more dispersed cell distribution observed here may be related to differences in matrix composition, including the lower alginate content used in our hydrogels. Strain-specific properties may also contribute, as non-motile *Synechocystis* strain used in this study has a reduced tendency to form cell aggregates or flocs (52), which could influence its spatial organisation within the matrix compared with motile lineages of *Synechocystis*.

2.2 Global evaluation of the proteome in immobilized cells

Next, label-free quantitative proteomic analysis was performed to investigate proteome remodelling in *Synechocystis* cells immobilised within the alginate hydrogel film relative to suspension cultures at three time points: days 1, 14, and 21. Because suspension cultures showed a noticeable decline in photosynthetic activity over extended cultivation (Fig. 2), the day 1 suspension culture was used as a control for the day 1 immobilized cells, while the day 14 suspension culture served as the control for both the day 14 and day 21 immobilized cultures (Fig. 1). This comparison strategy avoided using the physiologically deteriorated day 21 suspension cultures as a reference.

A total of 2981 proteins were identified, corresponding to approximately 80% of the predicted proteome, with each protein supported by at least two unique peptides (Table S1). Principal component analysis (PCA) revealed that the first and second components accounted for 59.7% and 17% of the total proteomic variation, respectively (Fig. 4A). The first component primarily distinguished younger cultures (day 1) from older cultures (days 14 and 21), while the second component separated immobilized samples from their suspension references. Differential abundance analysis identified 170, 543, and 586 significantly altered proteins in the day 1, day 14, and day 21 comparisons, respectively (Fig. 4B, Tables S2 and S3). The larger number of altered proteins at the later time points suggest that the proteomic differences between immobilized and suspension cells became more extensive during prolonged cultivation. However, 441 differentially abundant proteins were shared between the day 14 and day 21 comparisons (Fig. 4B), and broadly similar abundance patterns were observed for many proteins at these time points (Fig. 4D and 4E). Together, these findings suggest that much of the later-stage proteome remodelling had already been established by day 14 and was subsequently maintained through day 21.

As shown in Fig. 4F, Gene ontology (GO) enrichment analysis of proteins with increased abundance in hydrogel-entrapped cells revealed a clear temporal progression in the cellular response of *Synechocystis* to immobilization. Compared with the corresponding suspension cultures, the differentially expressed proteins in immobilized cells were significantly enriched ($p < 0.05$) in several GO terms spanning the categories of biological process (BP), cellular component (CC) and molecular function (MF) categories. At day 1, enrichment was primarily associated with stress-response functions, including iron-sulphur cluster binding, oxidoreductase activity, cell wall organization and transport pathways, indicating an early response aimed at maintaining redox homeostasis and protecting the photosynthetic apparatus. By day 14, the enrichment profile shifted toward RNA processing, carbon fixation, aerobic respiration, including terminal oxidases, and antiviral defence mechanisms including CRISPR-associated proteins, suggesting extensive metabolic adjustment and regulatory reprogramming under immobilized conditions. In addition, chlorophyll biosynthetic processes became significantly enriched, highlighting adaptations in photosynthetic machinery. Interestingly, proteins associated with iron-sulfur cluster binding remained enriched at all time points, suggesting their importance during immobilization. The GO enrichment pattern observed at day 21 largely resembled that at day 14, indicating a stabilised physiological state following initial adaptation. Together, these results illustrate a phased transition from an acute stress response to extensive physiological and metabolic remodelling during prolonged immobilization.

2.3 Proteome wide reprogramming reflects a shift from growth to maintenance

Comparative proteomics revealed extensive and time-dependent changes in protein abundance during immobilization, with cells remodelling their light harvesting and photosynthetic electron transfer routes. Although Chl *a* biosynthesis was upregulated, PSI and PSII core subunit levels remained largely unchanged (Fig. 5), indicating that the steady-state abundance of photosystem core proteins was maintained rather than increased. The increased abundance of the PSII assembly factor Sll0933 (53) suggests ongoing PSII assembly or repair-related turnover, consistent with the concurrent rise in proteins associated with Chl *a* biosynthesis. In contrast, Psb28-2 associates with fully assembled PSII rather than assembly intermediates, where it has been linked to restricting Q_A^--to-Q_B electron transfer (54). Its increased abundance may therefore reflect a regulatory or protective response associated with existing PSII complexes rather than a biogenesis-related process.

Cells also upregulated alternative electron sinks, respiratory pathways, and alternative ferredoxin isoforms. *Synechocystis* possesses 12 ferredoxin isoforms (Fed1–Fed12), although only little is known about their specific functions and potential functional redundancy (55). Fed1 is the highly abundant isoform essential for photosynthetic electron transport, and its abundance remained unchanged in our dataset, consistent with its role as the core, constitutively required ferredoxin. In contrast, four low-abundance isoforms - Fed2, Fed3, Fed5, and Fed7 - showed increased accumulation levels. Among the functionally characterized isoforms, Fed7 has been linked to photooxidative stress responses and is induced under low CO_2 and high-light conditions (56). Fed3 has been shown to support aerobic photomixotrophic growth together with Fed9 and pyruvate:ferredoxin oxidoreductase, though Fed9 itself was not upregulated here (57). The specific role of Fed5 remains unclear and requires further investigation.

Subunits representing all three respiratory terminal oxidases were more abundant in hydrogel-entrapped cells (Fig. 5). In *Synechocystis*, the aa3-type cytochrome c oxidase (COX), encoded by *ctaCIDIEI*, and the cytochrome *bd* quinol oxidase (Cyd), encoded by *cydAB*, are both confirmed as terminal oxidases of the thylakoid membrane, with Cyd potentially also present in the cytoplasmic membrane. In contrast, the alternative respiratory terminal oxidase (ARTO), encoded by *ctaCIIDIIEII*, has been localised exclusively to the cytoplasmic membrane (58, 59). The increased abundance of terminal oxidases suggests an enhanced capacity for respiratory electron flow to oxygen, potentially supporting proton-motive force generation and ATP synthesis and to some extent relieving over-reduction of the photosynthetic electron transport chain. NdbA, one of the three type 2 NAD(P)H dehydrogenases (NDH-2) in *Synechocystis*, showed higher abundance already after one day of immobilization. The thylakoid-localized NdbA transfers electrons from NADH to PQ pool (60, 61). Taken together, the upregulation of terminal oxidases and NdbA points to a broad enhancement of respiratory capacity during immobilization.

The flavodiiron (Flv) Flv1/Flv3 hetero-oligomer mediates photoreduction of O_2 downstream of PSI, and in contrast to the classical Mehler reaction occurring in chloroplasts, this transfer of electrons to O_2 happens without the formation of reactive oxygen species and produces only water (62–64). Under high CO_2 conditions such as the 3% CO_2 used here, the Flv1/Flv3 heterodimer is solely responsible for efficient steady-state O_2 photoreduction, with *flv2* and *flv4* expression strongly downregulated. The increased abundance of Flv3 in immobilised cells therefore suggests enhanced photoprotective electron flow to O_2 *via* the Mehler-like reaction, or alternatively *via* the Flv3 homo-oligomer. Homo-oligomers of Flv3 are involved in alternative electron transfer pathway(s) where the terminal acceptor is not O_2, but still remains to be identified, making Flv3 a more important player than Flv1 in the systems-wide acclimation of *Synechocystis* cells to stress (65).

In addition, subunits and maturation factors of the bidirectional [Ni-Fe] hydrogenase showed increased abundance (Fig. 5). This enzyme is linked to cellular redox metabolism and is favoured under reducing conditions (66). Therefore, its increased abundance may reflect the development of locally reducing and/or O_2-limited microenvironments within the alginate matrix, particularly in shaded interior regions of the dense hydrogel film where light penetration is limited (Fig. 3C and 3F) and respiratory O_2 consumption may exceed local photosynthetic O_2 production. However, because NifJ decreased in abundance, the proteomic data do not fully support a broad activation of fermentative metabolism in immobilized cells (67). Thus, the hydrogenase response is better interpreted as part of a broader reorganization of redox-balancing pathways rather than direct evidence for a fully anaerobic or fermentative state. This interpretation is consistent with previous studies showing that immobilization matrices can generate strong local gradients in oxygen, nutrients, and metabolic activity. For example, in agar gel-entrapped *Pseudomonas aeruginosa*, the anaerobically induced porin OprE was among the most strongly overexpressed proteins, indicating that oxygen-limited zones can develop within immobilized microbial systems (68). More generally, restricted mass transfer within immobilization matrices is known to create heterogeneous microenvironments rather than uniform physiological states across the whole cell population (35, 69).

Although cells were grown under 3% CO_2, where the CCM is typically supressed and growth is expected to be largely supported by passive diffusion of Ci, proteins involved in active Ci uptake were found at higher abundance in immobilized cells. In *Synechocystis*, BCT1 and SbtA are inducible high-affinity HCO_3^- transporters, while NDH-1_4 is a constitutive low-affinity CO_2 uptake system and NDH-1_3 is a high-affinity counterpart inducible specifically under Ci-limiting conditions. The upregulation of these transporters, particularly the low-Ci-inducible NDH-1_3, despite the high external CO_2 supply strongly suggests that cells within the alginate matrix may experience local Ci limitation due to restricted mass transfer. However, carboxysome proteins and Rubisco subunits were less abundant in the films, pointing to a decoupling between increased Ci acquisition capacity and carbon fixation output. This may reflect the growth-limited state, in which immobilized wild-type cells lack an efficient product-forming carbon sink beyond biomass accumulation. Under these conditions, increased Ci uptake capacity may support local Ci homeostasis rather than increased carbon fixation, while the reduced demand for biomass production

could explain the lower abundance of Rubisco and carboxysome components. Consistent with this interpretation, proteins associated with PHB metabolism, including PhaB and PhaE, increased in abundance at later time points, suggesting that immobilized cells may redirect part of the assimilated carbon and reducing power toward storage and redox-buffering pathways rather than growth.

- **2.4 Global downshift of protein synthesis may be orchestrated by the master regulator (p)ppGpp, linked to a longevity phenotype**

SpoT (Slr1325), a crucial bifunctional enzyme responsible for both the synthesis and degradation of the signalling molecules guanosine tetra- and penta-phosphate (collectively (p)ppGpp), showed higher accumulation in immobilised cells at days 14 and 21. These phosphorylated nucleotides mediate the conserved stringent response to environmental stresses in bacteria, including cyanobacteria, by regulating bacterial transcription and translation to reduce growth and promote stress acclimation (70–73). In many bacteria, the concentration of (p)ppGpp increases upon growth arrest leading to inhibition of the transcription of ribosomal genes (74–76). In *Synechococcus elongatus*, high (p)ppGpp levels have been shown to be involved to acclimation to darkness by slowing down DNA replication and preventing cell division in the dark (77). Moreover, the SpoT gene was found essential for *Rhodopseudomonas palustris* longevity when its growth is arrested (76, 78), and another (p)ppGpp synthase, RelA, was found important for transient growth-arrest in *E. coli* (74). As growth arrest and (p)ppGpp levels are important factors in natural biofilm formation (79), clear increase in SpoT abundance in the hydrogel embedded cells may indicate involvement of (p)ppGpp levels in the longevity of immobilised *Synechocystis* cells. Furthermore, regulation *via* SpoT is in agreement with the reduction of most of the ribosomal proteins (Fig. 5).

Immobilized cells contained fewer ribosomal proteins, chaperones and translation factors (Fig. 5). Enzymes involved in Fe-S cluster biosynthesis (NifU, NifS1-2) were also less abundant. Even though this clear downshift of protein synthesis capacity was evident, enzymes involved in amino acid biosynthesis were not coordinately diminished. While enzymes in histidine and threonine pathways showed lower abundance, enzymes in the branched-chain amino acid pathways (leucine and isoleucine), as well as cysteine and glutamate routes, were more abundant. Branched-chain amino acids can serve as a carbon and nitrogen source during starvation, which may indicate stationary phase-like behaviour in immobilised cells.

Among ion transporters, proteins associated with sulphate and potassium uptake were found in lower abundance in immobilized cells. As sulphur is used mainly for cysteine/methionine synthesis and select cofactors, lower demand for its uptake indicates reduced *de novo* protein synthesis under growth-limited conditions. Reduced demand for potassium points to lower translational activity, since ribosomes bind a substantial fraction of total Mg^{2+} and K^{+} (80). In contrast, higher iron and zinc uptake may reflect the higher abundance of iron rich terminal oxidases (which bind heme) and alternative ferredoxins (which bind FeS clusters), as well as zinc-dependent enzymes such as thylakoid-located carbonic anhydrase EcaB (Slr0051) suggested to interact functionally with the CupA/CupB CO_2 uptake systems (81).

Non-essential group 2 sigma factors have been shown to play important roles in acclimation to environmental changes (82–84). Among these, three group 2 sigma factors (SigB, SigD and SigE) were found in lower abundance, while the group 3 sigma factor SigF showed increased abundance. SigF has previously been linked to pilus formation (85).

2.5 Pilus and exopolysaccharide remodelling reinforces cell entrapment within the immobilization matrix

Proteins related to the cell surface, namely, the type IV pilus components PilC, PilN, PilO, and PilQ, were more abundant in immobilized cells. Cyanobacterial Type IV pili span the cell envelope and are responsible for motility, transformation competence, cell aggregation and secretion (86, 87). The non-motile glucose tolerant *Synechocystis* strain used in this study cannot form the thick pili required for motility, due to a loss of function mutation in the motality-regulating kinase SpkA (88, 89). Nonetheless, the cells retain the ability to form thin pili that serve other functions, such as DNA uptake or surface interaction. These thin pili are likely composed of minor pilins, but their exact role remain unclear (90, 91). Here, several minor pili proteins encoded from three different transcriptional units (*pilA5-6*, *pilA7* and *pilA9-11*) were upregulated in immobilised cells. In addition, another set of minor pilins, PilX1-3, was present at higher abundance in films (Fig. 5). PilX pili have been shown to facilitate flocculation, defined as the aggregation of planktonic cells into floating clusters (92). Although type IV pili were proposed to mediate direct extracellular electron transfer in *Synechocystis*, recent studies instead support an indirect, mediator-based mechanism, with pili contributing mainly to cell-electrode adhesion (93, 94). This suggests that minor pilin upregulation in immobilized cells may enhance scaffold attachment and biofilm-like cohesion relevant to biocatalyst stability.

A XxsE protein involved in the formation of synechan, a sulfated exopolysaccharide (95), also showed increased abundance. The genes encoding proteins involved in synechan synthesis and regulation, are located on the pSYSM plasmid in a cluster (*sll5042-sll5060*), with one additional gene located on the chromosome (*sll1581*). Most of these proteins, as well as another exopolysaccharide export protein, Wzc (Sll0923), showed enhanced abundance, but they did not meet our significance criteria. These findings suggest that even within an artificial scaffold, cells increase secretion of extracellular polymeric substances to reinforce their entrapment and physical retention within the immobilised matrix.

Long-term immobilization was also associated with a shift in protein translocation pathway usage: TatB, a key component of the twin-arginine translocation (Tat) pathway, was less abundant, while SecB, involved in general secretion (Sec) pathway, was more abundant. The Tat pathway is particularly important for transporting folded, cofactor-containing proteins, so its reduced abundance may point to decreased transport of folded proteins into the thylakoid lumen. The Sec pathway, in contrast, handles wide variety of unfolded proteins for translocation. Considering that pilins are co-translationally inserted into the membrane via the Sec pathway during pilin biogenesis (87), the increased abundance of Sec pathway components is in agreement with the elevated pilin levels observed in immobilised cells.

As immobilized cells showed only limited Chl *a* increase over the course of the experiment, cell division was also expected to be restricted (Fig. 2A). Intriguingly, Maf (Sll0905), which presumably inhibits synthesis of the division septum, increased in abundance in the immobilized cells (96). In contrasts, the peptidoglycan polymerases FtsW and FtsI, which produce septal peptidoglycan during cell division, were also more abundant in immobilized cultures (97). Together, these findings suggest that the division machinery remains in a poised, ready to resume state rather than fully arrested. Consistent with this, outgrowth was observed from the surface of the immobilized cultures, although these outgrowing cells were not harvested for the proteomic analysis.

2.6 Toxin-antitoxin system remodelling suggests a programmed cell death strategy in immobilized cultures

Although regulated cell death and programmed cell death (PCD)-like processes have been proposed in cyanobacteria, direct molecular evidence has remained limited (98). Recent work demonstrated that the underlying machinery is evolutionarily ancient and conserved well beyond animal, showing that a unicellular alga can show an apoptosis-like death pathway (99). This suggests that PCD machinery in photosynthetic microorganisms is more conserved and functionally relevant than previously thought, supporting the possibility that toxin-antitoxin (TA) -system-mediated cell death may contribute to population-level survival strategies in immobilized cultures. In bacteria, type II toxin-antitoxin (TA) systems are among the best-characterized molecular mediators involved in plasmid maintenance, biofilm formation, and, in some cases, stress-induced PCD-like processes (100, 101).

The *Synechocystis* genome encodes approximately 69 type II TA protein complexes (102), of which our proteomics analysis detected 41 toxins and 51 antitoxins; 23 of those showed significantly different abundance between immobilized and suspension cultures in at least one time point. Among these, the TA-pair YoeB-YefM, encoded at the Ssr0761 locus, is particularly notable, since both toxin and antitoxin increased in abundance specifically under long-term immobilization (Fig. 6). YoeB-YefM TA complex is a widespread type II TA system among archaea and bacteria, with reported roles in biofilm formation and stress responses, including oxidative stress (103). Its increased abundance in immobilized cells may therefore reflect activation of stress-adaptive TA modules under the spatially heterogeneous conditions of the immobilization matrix. In high dense photosynthetic films, surface-exposed cells may experience photooxidative stress, whereas shaded interior regions may become relatively more reducing. In addition, three plasmid (pSYSM) encoded toxins (Slr5102-Slr5101, Slr5017-Slr5018, and Sll5003-Sll5004) showed increased abundance under long-term immobilization, while their counterpart antitoxins were either reduced or unchanged. Although, the function of these specific modules remains uncharacterised, plasmid-encoded TA systems are known to contribute to plasmid stability through the post-segregational killing (102), and TA modules more broadly can participate in stress adaptation, and PCD-like processes (100, 104).

Taken together, the shift toward toxin excess relative to antitoxin abundance in long-term immobilized cultures is consistent with activation of TA-system components during prolonged immobilization. The

high photosynthetic activity, increase in Ci uptake and other adaptive pathways further indicate that immobilized cells remain metabolically active and argues against widespread cell death as the dominant response. Therefore, TA-system remodelling could be interpreted as part of a broader stress-adaptive programme that may support growth limitation and population-level stability within the heterogeneous hydrogel matrix, rather than as direct evidence for PCD-mediated nutrient recycling.

3 Conclusions

We show that physical entrapment of *Synechocystis* sp. PCC 6803 within thin Ca^{2+}-alginate hydrogel films induces a distinct physiological state that sustains photosynthetic activity while suppressing growth. Proteome-wide reprogramming reveals extensive, time-dependent rewiring of cellular metabolism in immobilized cells. Early responses emphasized redox stabilization and stress mitigation, whereas later time points showed enhanced photoprotective mechanisms, increased abundance of alternative electron sinks and respiratory terminal oxidases and upregulation of Ci uptake systems. Concomitant reduction in translational capacity, together with accumulation of the stringent-response regulator SpoT, suggests that (p)ppGpp signalling underpins this transition to a slow-growth, stress-tolerant high longevity state.

These features collectively resemble a biofilm-like metabolic mode shaped by diffusion limitation and spatial confinement yet remain distinct from classical stationary phase. We propose that immobilization actively drives cyanobacterial cells into a resource-efficient configuration optimized for long-term function rather than proliferation.

This work provides a mechanistic framework for microbial longevity in photosynthetic living materials and establishes immobilized cyanobacteria as robust platforms for sustained, energy-efficient photosynthetic biocatalysis.

Declarations

Ethics approval and consent to participate

Not applicable

Consent for publication

Not applicable

Competing interests

The authors declare that they have no competing interests

Funding

This research was supported by the European Commission (Solar to Butanol project #101172911), and Jane and Aatos Erkko Foundation (PhotoFactory #230042). HM's salary was also partly supported by the University of Turku Profi 7 SUSMAT program (#352727). Disclaimer: Views and opinions expressed are however those of the author(s) only and do not necessarily reflect those of the European Union. Neither the European Union nor the granting authority can be held responsible for them.

Author Contribution

YA conceived the study. HM, SK and YA designed the study. HM performed all the experiments, the data analysis and drafted the manuscript. SK performed the cell immobilization. EM assisted with the microscopy experiments. All authors contributed to the revision and finalization of the manuscript and approved the final version.

Acknowledgement

The authors would like to thank Samuel Svärd (University of Turku, Doctoral researcher) for technical assistance with the microtome.

Data Availability

All data supporting the findings of this study are available within the paper and its Supplementary Information. The proteomics datasets generated and analysed during the current study are available via PRIDE repository with the identifier PXD081286.

References

1. Agarwal P, Soni R, Kaur P, Madan A, Mishra R, Pandey J, et al. Cyanobacteria as a Promising Alternative for Sustainable Environment: Synthesis of Biofuel and Biodegradable Plastics. Front Microbiol. 2022;13. doi:10.3389/fmicb.2022.939347
2. Naduthodi MIS, Claassens NJ, D'Adamo S, van der Oost J, Barbosa MJ. Synthetic Biology Approaches To Enhance Microalgal Productivity. Trends in Biotechnology. 2021;39(10):1019–36. doi:10.1016/j.tibtech.2020.12.010
3. Toepel J, Karande R, Bühler B, Bühler K, Schmid A. Photosynthesis driven continuous hydrogen production by diazotrophic cyanobacteria in high cell density capillary photobiofilm reactors. Bioresource Technology. 2023;373:128703. doi:10.1016/j.biortech.2023.128703
4. Bozan M, Berreth H, Lindberg P, Bühler K. Cyanobacterial biofilms: from natural systems to applications. Trends in Biotechnology. 2025;43(2):318–32. doi:10.1016/j.tibtech.2024.08.005

5. Dranseike D, Cui Y, Ling AS, Donat F, Bernhard S, Bernero M, et al. Dual carbon sequestration with photosynthetic living materials. Nat Commun. 2025;16(1):3832. doi:10.1038/s41467-025-58761-y
6. Malihan-Yap L, Schmedler L, Pint D, Medipally H, Lackner F, Fedrigotti S, et al. Bioprinting of Nanocellulose Hydrogels for Photobiocatalysis Under Continuous Flow. ACS Sustainable Chem Eng. 2026;14(14):6599–612. doi:10.1021/acssuschemeng.5c09689
7. Taylor JE, Drake K, Tong N, Bezue JA, Nelson A, Atsumi S. Photosynthetic Biomanufacturing in Mechanically Robust, 3D Printed Hydrogels. ACS Synth Biol. 2025;14(11):4439–46. doi:10.1021/acssynbio.5c00366
8. Tóth GS, Backman O, Siivola T, Xu W, Kosourov S, Siitonen V, et al. Employing photocurable biopolymers to engineer photosynthetic 3D-printed living materials for production of chemicals. Green Chem. 2024;26(7):4032–42. doi:10.1039/D3GC04264B
9. Frenkel A, Zecharia E, Gómez-Pérez D, Sendersky E, Yegorov Y, Jacob A, et al. Cell specialization in cyanobacterial biofilm development revealed by expression of a cell-surface and extracellular matrix protein. npj Biofilms Microbiomes. 2023;9(1). doi:10.1038/s41522-023-00376-6
10. Bolhuis H, Cretoiu MS, Stal LJ. Molecular ecology of microbial mats. FEMS Microbiol Ecol. 2014;90(2):335–50. doi:10.1111/1574-6941.12408 PubMed PMID: 25109247.
11. Mager DM. Carbohydrates in cyanobacterial soil crusts as a source of carbon in the southwest Kalahari, Botswana. Soil Biology and Biochemistry. 2010;42(2):313–8. doi:10.1016/j.soilbio.2009.11.009
12. Rossi F, De Philippis R. Role of Cyanobacterial Exopolysaccharides in Phototrophic Biofilms and in Complex Microbial Mats. Life. 2015;5(2):2. doi:10.3390/life5021218
13. Stuart RK, Mayali X, Lee JZ, Craig Everroad R, Hwang M, Bebout BM, et al. Cyanobacterial reuse of extracellular organic carbon in microbial mats. The ISME Journal. 2016;10(5):1240–51. doi:10.1038/ismej.2015.180
14. Allen R, Rittmann BE, Curtiss R. Axenic Biofilm Formation and Aggregation by Synechocystis sp. Strain PCC 6803 Are Induced by Changes in Nutrient Concentration and Require Cell Surface Structures. Appl Environ Microbiol. 2019;85(7):e02192-18. doi:10.1128/AEM.02192-18 PubMed PMID: 30709828; PubMed Central PMCID: PMC6585507.
15. Pereira S, Zille A, Micheletti E, Moradas-Ferreira P, De Philippis R, Tamagnini P. Complexity of cyanobacterial exopolysaccharides: composition, structures, inducing factors and putative genes involved in their biosynthesis and assembly. FEMS Microbiol Rev. 2009;33(5):917–41. doi:10.1111/j.1574-6976.2009.00183.x PubMed PMID: 19453747.
16. Bertocchi C, Navarini L, Cesàro A, Anastasio M. Polysaccharides from cyanobacteria. Carbohydrate Polymers. 1990;12(2):127–53. doi:10.1016/0144-8617(90)90015-K
17. Flemming HC, van Hullebusch ED, Neu TR, Nielsen PH, Seviour T, Stoodley P, et al. The biofilm matrix: multitasking in a shared space. Nat Rev Microbiol. 2023;21(2):70–86. doi:10.1038/s41579-022-00791-0

18. Bozan M, Berreth H, Lindberg P, Bühler K. Cyanobacterial biofilms: from natural systems to applications. Trends in Biotechnology. 2025;43(2):318–32. doi:10.1016/j.tibtech.2024.08.005
19. Datta D, Weiss EL, Wangpraseurt D, Hild E, Chen S, Golden JW, et al. Phenotypically complex living materials containing engineered cyanobacteria. Nat Commun. 2023;14(1). doi:10.1038/s41467-023-40265-2
20. Rivera-Tarazona LK, Campbell ZT, Ware TH. Stimuli-responsive engineered living materials. Soft Matter. 2021;17(4):785–809. doi:10.1039/D0SM01905D
21. Kosourov S, Tammelin T, Allahverdiyeva Y. Engineered biocatalytic architecture for enhanced light utilisation in algal H2 production. Energy Environ Sci. 2025;18(2):937–47. doi:10.1039/D4EE03075C
22. Levä T, Rissanen V, Nikkanen L, Siitonen V, Heilala M, Phiri J, et al. Mapping Nanocellulose- and Alginate-Based Photosynthetic Cell Factory Scaffolds: Interlinking Porosity, Wet Strength, and Gas Exchange. Biomacromolecules. 2023;24(8):3484–97. doi:10.1021/acs.biomac.3c00261
23. Tóth GS, Backman O, Siivola T, Xu W, Kosourov S, Siitonen V, et al. Employing photocurable biopolymers to engineer photosynthetic 3D-printed living materials for production of chemicals. Green Chem. 2024;26(7):4032–42. doi:10.1039/D3GC04264B
24. Virkkala T, Kosourov S, Rissanen V, Siitonen V, Arola S, Allahverdiyeva Y, et al. Bioinspired mechanically stable all-polysaccharide based scaffold for photosynthetic production. J Mater Chem B. 2023;11(36):8788–803. doi:10.1039/d3tb00919j
25. Sugianto W, Altin-Yavuzarslan G, Tickman BI, Kiattisewee C, Yuan SF, Brooks SM, et al. Gene expression dynamics in input-responsive engineered living materials programmed for bioproduction. Materials Today Bio. 2023;20:100677. doi:10.1016/j.mtbio.2023.100677
26. Kosourov S, Leino H, Murukesan G, Lynch F, Sivonen K, Tsygankov AA, et al. Hydrogen Photoproduction by Immobilized N2-Fixing Cyanobacteria: Understanding the Role of the Uptake Hydrogenase in the Long-Term Process. Applied and Environmental Microbiology. 2014;80(18):5807–17. doi:10.1128/AEM.01776-14
27. Kosourov S, Siitonen V, Tóth G, Levä T, Tammelin T, Kallio P, et al. Over four months of ethylene production: Unlocking the potential of solid-state photosynthetic cell factories [Internet]. bioRxiv; 2025 [cited 2026 Jan 28]. p. 2025.09.12.675104. Available from: https://www.biorxiv.org/content/10.1101/2025.09.12.675104v1 doi:10.1101/2025.09.12.675104
28. Lee H, Shin D, Choi J, Ki CS, Hyun J. Mimicry of the plant leaf with a living hydrogel sheet of cellulose nanofibers. Carbohydrate Polymers. 2022;290:119485. doi:10.1016/j.carbpol.2022.119485
29. Vajravel S, Sirin S, Kosourov S, Allahverdiyeva Y. Towards sustainable ethylene production with cyanobacterial artificial biofilms. Green Chem. 2020;22(19):6404–14. doi:10.1039/D0GC01830A
30. Levä T, Mahlamäki E, Kosourov S, Allahverdiyeva Y, Mäkelä M, Tammelin T. Non-invasive monitoring of cyanobacteria growth in a nanocellulose matrix. Algal Research. 2025;89:104090. doi:10.1016/j.algal.2025.104090
31. Oh J, Ammu S, Vriend VD, Kieffer R, Kleiner FH, Balasubramanian S, et al. Growth, Distribution, and Photosynthesis of *Chlamydomonas Reinhardtii* in 3D Hydrogels. Advanced Materials. 2024;36(2).

doi:10.1002/adma.202305505

32. Wan N, Wang H, Ng CK, Mukherjee M, Ren D, Cao B, et al. Bacterial Metabolism During Biofilm Growth Investigated by 13C Tracing. Front Microbiol. 2018;9. doi:10.3389/fmicb.2018.02657
33. Żur J, Wojcieszyńska D, Guzik U. Metabolic Responses of Bacterial Cells to Immobilization. Molecules. 2016;21(7):958. doi:10.3390/molecules21070958
34. Junter GA, Coquet L, Vilain S, Jouenne T. Immobilized-cell physiology: current data and the potentialities of proteomics. Enzyme and Microbial Technology. 2002;31(3):201–12. doi:10.1016/s0141-0229(02)00073-x
35. Perrot F, Hébraud M, Charlionet R, Junter GA, Jouenne T. Protein patterns of gel-entrappedEscherichia coli cells differ from those of free-floating organisms. Electrophoresis. 2000;21(3):645–53. doi:10.1002/(sici)1522-2683(20000201)21:3%3C645::aid-elps645%3E3.0.co;2-1
36. Priks H, Butelmann T, Illarionov A, Johnston TG, Fellin C, Tamm T, et al. Physical Confinement Impacts Cellular Phenotypes within Living Materials. ACS Appl Bio Mater. 2020;3(7):4273–81. doi:10.1021/acsabm.0c00335
37. Yoshitomi T, Kaminaga S, Sato N, Toyoshima M, Moriyama T, Yoshimoto K. Formation of Spherical Palmelloid Colony with Enhanced Lipid Accumulation by Gel Encapsulation of Chlamydomonas debaryana NIES-2212. Plant and Cell Physiology. 2020;61(1):158–68. doi:10.1093/pcp/pcz188
38. Kosourov S, Siitonen V, Tóth G, Levä T, Tammelin T, Kallio P, et al. Over four months of ethylene production: Unlocking the potential of solid-state photosynthetic cell factories [Internet]. bioRxiv; 2025 [cited 2026 Jan 28]. p. 2025.09.12.675104. Available from: https://www.biorxiv.org/content/10.1101/2025.09.12.675104v1 doi:10.1101/2025.09.12.675104
39. Kosourov SN, Seibert M. Hydrogen photoproduction by nutrient-deprived Chlamydomonas reinhardtii cells immobilized within thin alginate films under aerobic and anaerobic conditions. Biotechnology and Bioengineering. 2009;102(1):50–8. doi:10.1002/bit.22050
40. Mustila H, Muth-Pawlak D, Aro E, Allahverdiyeva Y. Global proteomic response of unicellular cyanobacterium *Synechocystis* sp. PCC 6803 to fluctuating light upon CO_2 step-down. Physiologia Plantarum. 2021 Jun 30. doi:10.1111/ppl.13482
41. Mustila H, Muth-Pawlak D, Aro E, Allahverdiyeva Y. Global proteomic response of unicellular cyanobacterium *Synechocystis* sp. PCC 6803 to fluctuating light upon CO_2 step-down. Physiologia Plantarum. 2021 Jun 30. doi:10.1111/ppl.13482
42. Frankenfield AM, Ni J, Ahmed M, Hao L. Protein Contaminants Matter: Building Universal Protein Contaminant Libraries for DDA and DIA Proteomics. J Proteome Res. 2022;21(9):2104–13. doi:10.1021/acs.jproteome.2c00145
43. Perez-Riverol Y, Bandla C, Kundu DJ, Kamatchinathan S, Bai J, Hewapathirana S, et al. The PRIDE database at 20 years: 2025 update. Nucleic Acids Research. 2025;53(D1):D543–53. doi:10.1093/nar/gkae1011
44. Heberle H, Meirelles GV, da Silva FR, Telles GP, Minghim R. InteractiVenn: a web-based tool for the analysis of sets through Venn diagrams. BMC Bioinformatics. 2015;16(1):169. doi:10.1186/s12859-

015-0611-3

45. Kłodawska K, Kovács L, Vladkova R, Rzaska A, Gombos Z, Laczkó-Dobos H, et al. Trimeric organization of photosystem I is required to maintain the balanced photosynthetic electron flow in cyanobacterium Synechocystis sp. PCC 6803. Photosynth Res. 2020;143(3):251–62. doi:10.1007/s11120-019-00696-9
46. Rakhimberdieva MG, Vavilin DV, Vermaas WFJ, Elanskaya IV, Karapetyan NV. Phycobilin/chlorophyll excitation equilibration upon carotenoid-induced non-photochemical fluorescence quenching in phycobilisomes of the cyanobacterium *Synechocystis* sp. PCC 6803. Biochimica et Biophysica Acta (BBA) - Bioenergetics. 2007;Structure and Function of Photosystems1767(6):757–65. doi:10.1016/j.bbabio.2006.12.007
47. Tamary E, Kiss V, Nevo R, Adam Z, Bernát G, Rexroth S, et al. Structural and functional alterations of cyanobacterial phycobilisomes induced by high-light stress. Biochimica et Biophysica Acta (BBA) - Bioenergetics. 2012;1817(2):319–27. doi:10.1016/j.bbabio.2011.11.008
48. Tóth GS, Siitonen V, Nikkanen L, Sovic L, Kallio P, Kourist R, et al. Photosynthetically produced sucrose by immobilized Synechocystis sp. PCC 6803 drives biotransformation in E. coli. Biotechnol Biofuels. 2022;15(1). doi:10.1186/s13068-022-02248-1
49. Vajravel S, Sirin S, Kosourov S, Allahverdiyeva Y. Towards sustainable ethylene production with cyanobacterial artificial biofilms. Green Chem. 2020;22(19):6404–14. doi:10.1039/D0GC01830A
50. Tan X, Du W, Lu X. Photosynthetic and extracellular production of glucosylglycerol by genetically engineered and gel-encapsulated cyanobacteria. Appl Microbiol Biotechnol. 2015;99(5):2147–54. doi:10.1007/s00253-014-6273-7
51. Valsami EA, Pateraki A, Melis A, Ghanotakis DF. Heterologous β-phellandrene production by alginate immobilized Synechocystis sp. PCC 6803. J Appl Phycol. 2021;33(4):2157–68. doi:10.1007/s10811-021-02451-x
52. Conradi FD, Zhou RQ, Oeser S, Schuergers N, Wilde A, Mullineaux CW. Factors Controlling Floc Formation and Structure in the Cyanobacterium Synechocystis sp. Strain PCC 6803. J Bacteriol. 2019;201(19):e00344-19. doi:10.1128/JB.00344-19 PubMed PMID: 31262837; PubMed Central PMCID: PMC6755745.
53. Rengstl B, Knoppová J, Komenda J, Nickelsen J. Characterization of a Synechocystis double mutant lacking the photosystem II assembly factors YCF48 and Sll0933. Planta. 2013;237(2):471–80. doi:10.1007/s00425-012-1720-0
54. Huokko T, Sporre E, Koch B, Patil PP, Wey L, Nikkanen L, et al. Differences in photosystem II activity and carbon allocation during photomixotrophic growth in distinct wild-type strains of Synechocystis sp. PCC 6803. The Plant Journal. 2026;125(2):e70683. doi:10.1111/tpj.70683
55. Boehm M, Svedruzic D, Lubner CE, Appel J, Mulder DW, Kisgeropoulos EC, et al. Comprehensive study on ferredoxin isoforms in the cyanobacterium Synechocystis sp. PCC 6803 [Internet]. bioRxiv; 2026 [cited 2026 Jul 13]. p. 2026.04.08.717189. Available from: https://www.biorxiv.org/content/10.64898/2026.04.08.717189v1 doi:10.64898/2026.04.08.717189

56. Mustila H, Allahverdiyeva Y, Isojärvi J, Aro EM, Eisenhut M. The bacterial-type [4Fe–4S] ferredoxin 7 has a regulatory function under photooxidative stress conditions in the cyanobacterium Synechocystis sp. PCC 6803. Biochimica et Biophysica Acta (BBA) - Bioenergetics. 2014;1837(8):1293–304. doi:10.1016/j.bbabio.2014.04.006
57. Wang Y, Chen X, Spengler K, Terberger K, Boehm M, Appel J, et al. Pyruvate:ferredoxin oxidoreductase and low abundant ferredoxins support aerobic photomixotrophic growth in cyanobacteria. Kramer DM, Storz G, Ducat DC, Burnap R, Nitschke W, editors. eLife. 2022;11:e71339. doi:10.7554/eLife.71339
58. Howitt CA, Vermaas WF. Quinol and cytochrome oxidases in the cyanobacterium Synechocystis sp. PCC 6803. Biochemistry. 1998;37(51):17944–51. doi:10.1021/bi981486n PubMed PMID: 9922162.
59. Lea-Smith DJ, Bombelli P, Vasudevan R, Howe CJ. Photosynthetic, respiratory and extracellular electron transport pathways in cyanobacteria. Biochimica et Biophysica Acta (BBA) - Bioenergetics. 2016;Organization and dynamics of bioenergetic systems in bacteria1857(3):247–55. doi:10.1016/j.bbabio.2015.10.007
60. Howitt CA, Udall PK, Vermaas WF. Type 2 NADH dehydrogenases in the cyanobacterium Synechocystis sp. strain PCC 6803 are involved in regulation rather than respiration. J Bacteriol. 1999;181(13):3994–4003. doi:10.1128/JB.181.13.3994-4003.1999 PubMed PMID: 10383967; PubMed Central PMCID: PMC93889.
61. Huokko T, Muth-Pawlak D, Aro EM. Thylakoid Localized Type 2 NAD(P)H Dehydrogenase NdbA Optimizes Light-Activated Heterotrophic Growth of Synechocystis sp. PCC 6803. Plant Cell Physiol. 2019;60(6):1386–99. doi:10.1093/pcp/pcz044
62. Eckardt NA, Allahverdiyeva Y, Alvarez CE, Büchel C, Burlacot A, Cardona T, et al. Lighting the way: Compelling open questions in photosynthesis research. The Plant Cell. 2024;36(10):3914–43. doi:10.1093/plcell/koae203
63. Helman Y, Tchernov D, Reinhold L, Shibata M, Ogawa T, Schwarz R, et al. Genes encoding A-type flavoproteins are essential for photoreduction of O2 in cyanobacteria. Curr Biol. 2003;13(3):230–5. doi:10.1016/s0960-9822(03)00046-0 PubMed PMID: 12573219.
64. Vicente JB, Gomes CM, Wasserfallen A, Teixeira M. Module fusion in an A-type flavoprotein from the cyanobacterium *Synechocystis* condenses a multiple-component pathway in a single polypeptide chain. Biochemical and Biophysical Research Communications. 2002;294(1):82–7. doi:10.1016/S0006-291X(02)00434-5
65. Mustila H, Paananen P, Battchikova N, Santana-Sánchez A, Muth-Pawlak D, Hagemann M, et al. The Flavodiiron Protein Flv3 Functions as a Homo-Oligomer During Stress Acclimation and is Distinct from the Flv1/Flv3 Hetero-Oligomer Specific to the O_2Photoreduction Pathway. Plant Cell Physiol. 2016;pcw047. doi:10.1093/pcp/pcw047
66. Burgstaller H, Wang Y, Caliebe J, Hueren V, Appel J, Boehm M, et al. Synechocystis sp. PCC 6803 Requires the Bidirectional Hydrogenase to Metabolize Glucose and Arginine Under Oxic Conditions. Front Microbiol. 2022;13. doi:10.3389/fmicb.2022.896190

67. McNeely K, Xu Y, Ananyev G, Bennette N, Bryant DA, Dismukes GC. Synechococcus sp. Strain PCC 7002 nifJ Mutant Lacking Pyruvate:Ferredoxin Oxidoreductase. Applied and Environmental Microbiology. 2011;77(7):2435–44. doi:10.1128/AEM.02792-10
68. Vilain S, Cosette P, Hubert M, Lange C, Junter GA, Jouenne T. Proteomic analysis of agar gel-entrapped Pseudomonas aeruginosa. Proteomics. 2004;4(7):1996–2004. doi:10.1002/pmic.200300707
69. Junter GA, Jouenne T. Immobilized viable microbial cells: from the process to the proteome… or the cart before the horse. Biotechnology Advances. 2004;22(8):633–58. doi:10.1016/j.biotechadv.2004.06.003
70. Hidese R, Ohbayashi R, Kato Y, Matsuda M, Tanaka K, Imamura S, et al. ppGpp accumulation reduces the expression of the global nitrogen homeostasis-modulating NtcA regulon by affecting 2-oxoglutarate levels. Commun Biol. 2023;6(1):1285. doi:10.1038/s42003-023-05632-1
71. Mu H, Han F, Wang Q, Wang Y, Dai X, Zhu M. Recent functional insights into the magic role of (p)ppGpp in growth control. Computational and Structural Biotechnology Journal. 2023;21:168–75. doi:10.1016/j.csbj.2022.11.063
72. Ning D, Qian Y, Miao X, Wen C. Role of the all1549 (ana-rsh) Gene, A relA/spoT Homolog, of the Cyanobacterium Anabaena sp. PCC7120. Curr Microbiol. 2011;62(6):1767–73. doi:10.1007/s00284-011-9926-0
73. Surányi G, Korcz A, Pálfi Z, Borbély G. Effects of light deprivation on RNA synthesis, accumulation of guanosine 3’(2’)-diphosphate 5’-diphosphate, and protein synthesis in heat-shocked Synechococcus sp. strain PCC 6301, a cyanobacterium. Journal of Bacteriology. 1987;169(2):632–9. doi:10.1128/jb.169.2.632-639.1987
74. Bokinsky G, Baidoo EEK, Akella S, Burd H, Weaver D, Alonso-Gutierrez J, et al. HipA-triggered growth arrest and β-lactam tolerance in Escherichia coli are mediated by RelA-dependent ppGpp synthesis. J Bacteriol. 2013;195(14):3173–82. doi:10.1128/JB.02210-12 PubMed PMID: 23667235; PubMed Central PMCID: PMC3697643.
75. Hauryliuk V, Atkinson GC, Murakami KS, Tenson T, Gerdes K. Recent functional insights into the role of (p)ppGpp in bacterial physiology. Nat Rev Microbiol. 2015;13(5):298–309. doi:10.1038/nrmicro3448
76. Yin L, Ma H, Nakayasu ES, Payne SH, Morris DR, Harwood CS. Bacterial Longevity Requires Protein Synthesis and a Stringent Response. mBio. 2019;10(5):e02189-19. doi: 10.1128 /mBio.02189-19 PubMed PMID: 31615958; PubMed Central PMCID: PMC6794480.
77. Hood RD, Higgins SA, Flamholz A, Nichols RJ, Savage DF. The stringent response regulates adaptation to darkness in the cyanobacterium Synechococcus elongatus. Proceedings of the National Academy of Sciences. 2016;113(33):E4867–76. doi:10.1073/pnas.1524915113
78. Pechter KB, Yin L, Oda Y, Gallagher L, Yang J, Manoil C, et al. Molecular Basis of Bacterial Longevity. mBio. 2017;8(6):10.1128/mbio.01726-17. doi:10.1128/mbio.01726-17

79. Engelhardt F, Turnbull K, Gür M, Müsken M, Preusse M, Häussler S, et al. (p)ppGpp imposes graded transcriptional changes to impair motility and promote antibiotic tolerance in biofilms. npj Biofilms Microbiomes. 2025;11(1):148. doi:10.1038/s41522-025-00795-7
80. Nierhaus KH. Mg2+, K+, and the ribosome. J Bacteriol. 2014;196(22):3817–9. doi: 10.1128
/JB.02297-14 PubMed PMID: 25225274; PubMed Central PMCID: PMC4248827.
81. Sun N, Han X, Xu M, Kaplan A, Espie GS, Mi H. A thylakoid-located carbonic anhydrase regulates CO2 uptake in the cyanobacterium Synechocystis sp. PCC 6803. New Phytologist. 2019;222(1):206–17. doi:10.1111/nph.15575
82. Srivastava A, Summers ML, Sobotka R. Cyanobacterial sigma factors: Current and future applications for biotechnological advances. Biotechnology Advances. 2020;40:107517. doi:10.1016/j.biotechadv.2020.107517
83. Turunen O, Koskinen S, Kurkela J, Karhuvaara O, Hakkila K, Tyystjärvi T. Roles of Close Homologues SigB and SigD in Heat and High Light Acclimation of the Cyanobacterium Synechocystis sp. PCC 6803. Life (Basel). 2022;12(2):162. doi:10.3390/life12020162 PubMed PMID: 35207450; PubMed Central PMCID: PMC8875361.
84. Tyystjärvi T, Huokko T, Rantamäki S, Tyystjärvi E. Impact of Different Group 2 Sigma Factors on Light Use Efficiency and High Salt Stress in the Cyanobacterium Synechocystis sp. PCC 6803. PLOS ONE. 2013;8(4):e63020. doi:10.1371/journal.pone.0063020
85. Bhaya D, Watanabe N, Ogawa T, Grossman AR. The role of an alternative sigma factor in motility and pilus formation in the cyanobacterium Synechocystis sp. strain PCC6803. Proceedings of the National Academy of Sciences. 1999;96(6):3188–93. doi:10.1073/pnas.96.6.3188
86. Hammerl J, Schuergers N, Enomoto G, Mullineaux CW, Wilde A. Beyond movement: the dynamic roles of Type IV pili in cyanobacterial life. O'Toole G, editor. J Bacteriol. 2025;207(7). doi:10.1128/jb.00086-25
87. Linhartová M, Bučinská L, Halada P, Ječmen T, Šetlík J, Komenda J, et al. Accumulation of the Type IV prepilin triggers degradation of SecY and YidC and inhibits synthesis of Photosystem II proteins in the cyanobacterium Synechocystis PCC 6803. Molecular Microbiology. 2014;93(6):1207–23. doi:10.1111/mmi.12730
88. Koskinen S, Kurkela J, Linhartová M, Tyystjärvi T. The genome sequence of *Synechocystis* sp. PCC 6803 substrain GT-T and its implications for the evolution of PCC 6803 substrains. FEBS Open Bio. 2023;13(4):701–12. doi:10.1002/2211-5463.13576
89. Panichkin VB, Arakawa-Kobayashi S, Kanaseki T, Suzuki I, Los DA, Shestakov SV, et al. Serine/Threonine Protein Kinase SpkA in *Synechocystis* sp. Strain PCC 6803 Is a Regulator of Expression of Three Putative *pilA* Operons, Formation of Thick Pili, and Cell Motility. J Bacteriol. 2006;188(21):7696–9. doi:10.1128/JB.00838-06
90. Bhaya D, Bianco NR, Bryant D, Grossman A. Type IV pilus biogenesis and motility in the cyanobacterium *Synechocystis* sp. PCC6803. Molecular Microbiology. 2000;37(4):941–51.

doi:10.1046/j.1365-2958.2000.02068.x

91. Chen Z, Li X, Tan X, Zhang Y, Wang B. Recent Advances in Biological Functions of Thick Pili in the Cyanobacterium Synechocystis sp. PCC 6803. Front Plant Sci. 2020;11:241. doi:10.3389/fpls.2020.00241
92. Oeser S, Wallner T, Schuergers N, Bučinská L, Sivabalasarma S, Bähre H, et al. Minor pilins are involved in motility and natural competence in the cyanobacterium *Synechocystis* sp. PCC 6803. Molecular Microbiology. 2021;116(3):743–65. doi:10.1111/mmi.14768
93. Thirumurthy MA, Hitchcock A, Cereda A, Liu J, Chavez MS, Doss BL, et al. Type IV Pili-Independent Photocurrent Production by the Cyanobacterium Synechocystis sp. PCC 6803. Front Microbiol. 2020;11. doi:10.3389/fmicb.2020.01344
94. Wey LT, Lawrence JM, Chen X, Clark R, Lea-Smith DJ, Zhang JZ, et al. A biophotoelectrochemical approach to unravelling the role of cyanobacterial cell structures in exoelectrogenesis. Electrochimica Acta. 2021;395:139214. doi:10.1016/j.electacta.2021.139214
95. Maeda K, Okuda Y, Enomoto G, Watanabe S, Ikeuchi M. Biosynthesis of a sulfated exopolysaccharide, synechan, and bloom formation in the model cyanobacterium Synechocystis sp. strain PCC 6803. eLife. 2021;10. doi:10.7554/elife.66538
96. Hamoen LW. Cell division blockage: but this time by a surprisingly conserved protein. Molecular Microbiology. 2011;81(1):1–3. doi:10.1111/j.1365-2958.2011.07693.x
97. Taguchi A, Welsh MA, Marmont LS, Lee W, Sjodt M, Kruse AC, et al. FtsW is a peptidoglycan polymerase that is functional only in complex with its cognate penicillin-binding protein. Nat Microbiol. 2019;4(4):587–94. doi:10.1038/s41564-018-0345-x
98. Aguilera A, Klemenčič M, Sueldo DJ, Rzymski P, Giannuzzi L, Martin MV. Cell Death in Cyanobacteria: Current Understanding and Recommendations for a Consensus on Its Nomenclature. Front Microbiol. 2021;12. doi:10.3389/fmicb.2021.631654
99. Corredor L, Vergou GA, Skalický V, Antoniadi I, Wheaton BJ, Ljung K, et al. Apoptotic bodies in phytoplankton suggest evolutionary conservation of cell death mechanisms. Nat Commun. 2025;16(1). doi:10.1038/s41467-025-63956-4
100. Aguilera A, Klemenčič M, Sueldo DJ, Rzymski P, Giannuzzi L, Martin MV. Cell Death in Cyanobacteria: Current Understanding and Recommendations for a Consensus on Its Nomenclature. Front Microbiol. 2021;12. doi:10.3389/fmicb.2021.631654
101. Srikumar A, Krishna PS, Sivaramakrishna D, Kopfmann S, Hess WR, Swamy MJ, et al. The Ssl2245-Sll1130 Toxin-Antitoxin System Mediates Heat-induced Programmed Cell Death in Synechocystis sp. PCC6803. Journal of Biological Chemistry. 2017;292(10):4222–34. doi:10.1074/jbc.m116.748178
102. Kopfmann S, Roesch S, Hess W. Type II Toxin–Antitoxin Systems in the Unicellular Cyanobacterium Synechocystis sp. PCC 6803. Toxins. 2016;8(7):228. doi:10.3390/toxins8070228
103. Chan WT, Domenech M, Moreno-Córdoba I, Navarro-Martínez V, Nieto C, Moscoso M, et al. The Streptococcus pneumoniae yefM-yoeB and relBE Toxin-Antitoxin Operons Participate in Oxidative

Stress and Biofilm Formation. Toxins. 2018;10(9):378. doi:10.3390/toxins10090378

104. Srikumar A, Krishna PS, Sivaramakrishna D, Kopfmann S, Hess WR, Swamy MJ, et al. The Ssl2245-Sll1130 Toxin-Antitoxin System Mediates Heat-induced Programmed Cell Death in Synechocystis sp. PCC6803. Journal of Biological Chemistry. 2017;292(10):4222–34. doi:10.1074/jbc.m116.748178

105. Kopfmann S, Roesch S, Hess W. Type II Toxin–Antitoxin Systems in the Unicellular Cyanobacterium Synechocystis sp. PCC 6803. Toxins. 2016;8(7):228. doi:10.3390/toxins8070228

Figures

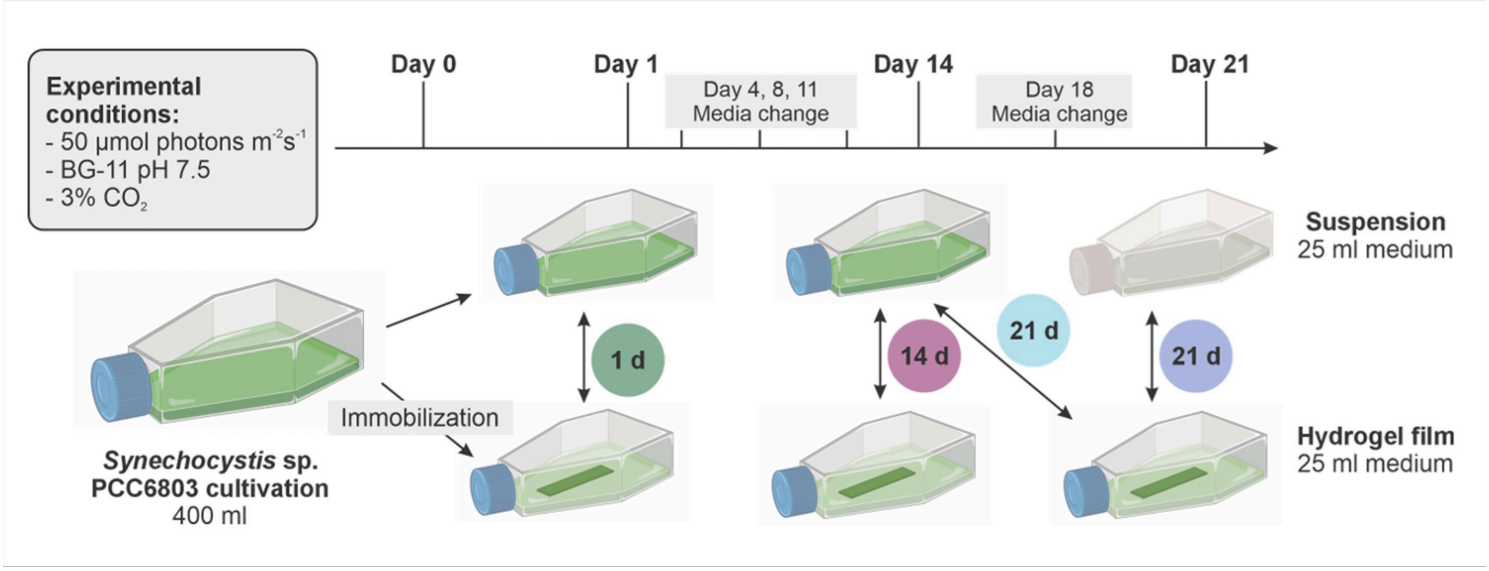

Figure 1

Schematic overview of the experimental workflow for physiological and proteomic profiling of suspension and immobilized *Synechocystis*. Samples for proteome analysis were collected from suspension cultures on days 1 and 14 only, as suspension cultures exhibited very low photosynthetic activity on day 21. Proteome samples from immobilized cells were collected on days 1, 14, and 21. Physiological measurements were performed on both suspension and immobilized cultures at days 1, 14, and 21.

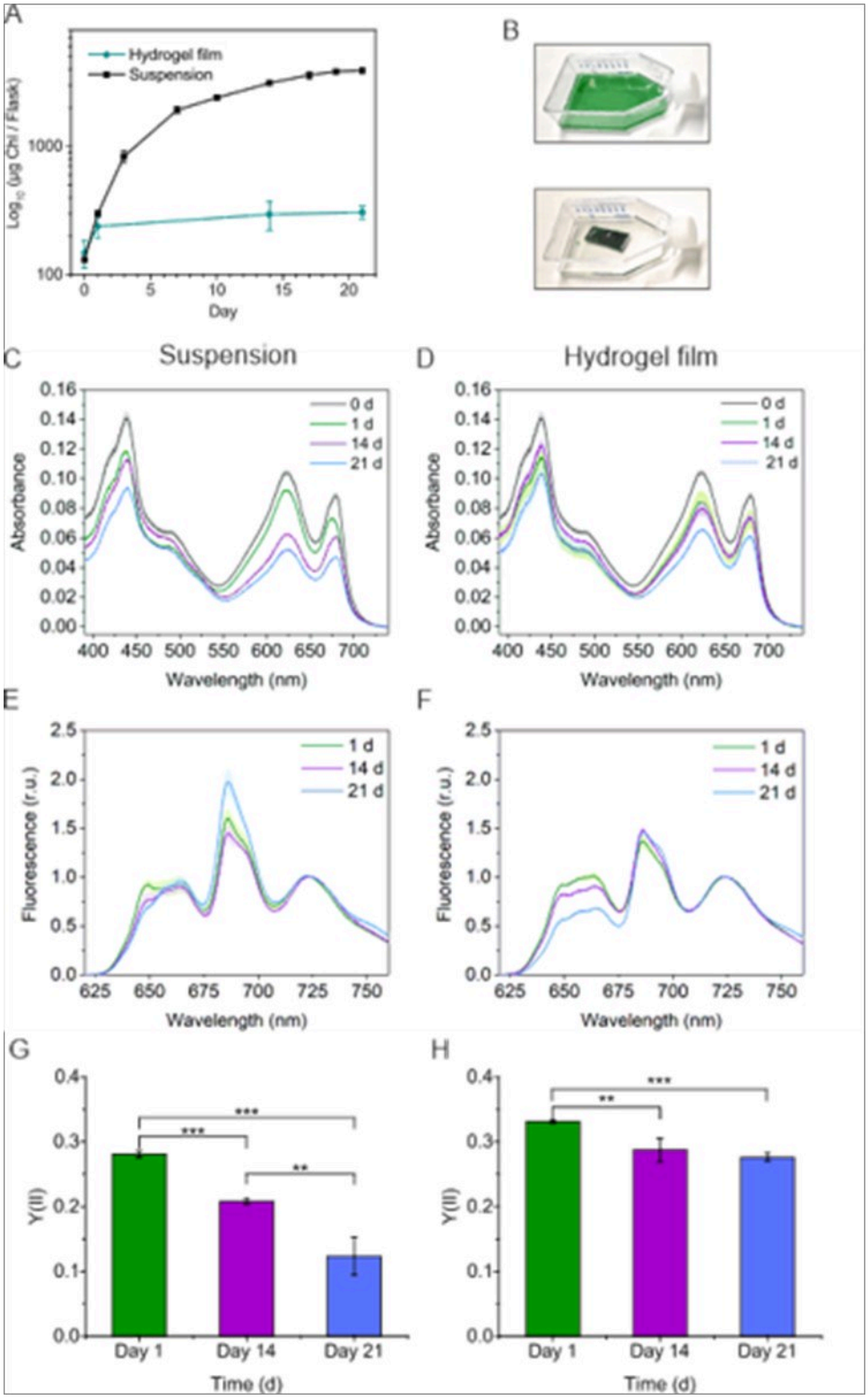

Figure 2

Growth, pigments and photosynthetic properties of suspension and immobilised cells in hydrogel films. (A) Growth of *Synechocystis*assessed based on Chl *a* content. (B) Suspension and immobilized cells in hydrogel films (on day 1 of cultivation). In *vivo* absorption spectra measured from suspension cultures (C) and hydrogel films (D). 77 K fluorescence spectra, excited with phycobilisome specific light at 580 nm, from suspension cultures (E) and hydrogel films (F), the graphs were normalized to Photosystem I

fluorescence peak at 725 nm. The effective yield of PSII (Y(II)) was determined by applying saturating pulses during fluorescence induction curve in suspension cultures (G) and hydrogel films (H). Y(II) value shown was taken at 300 s of illumination. Values are means ± SD; n = 3–4 biological replicates.

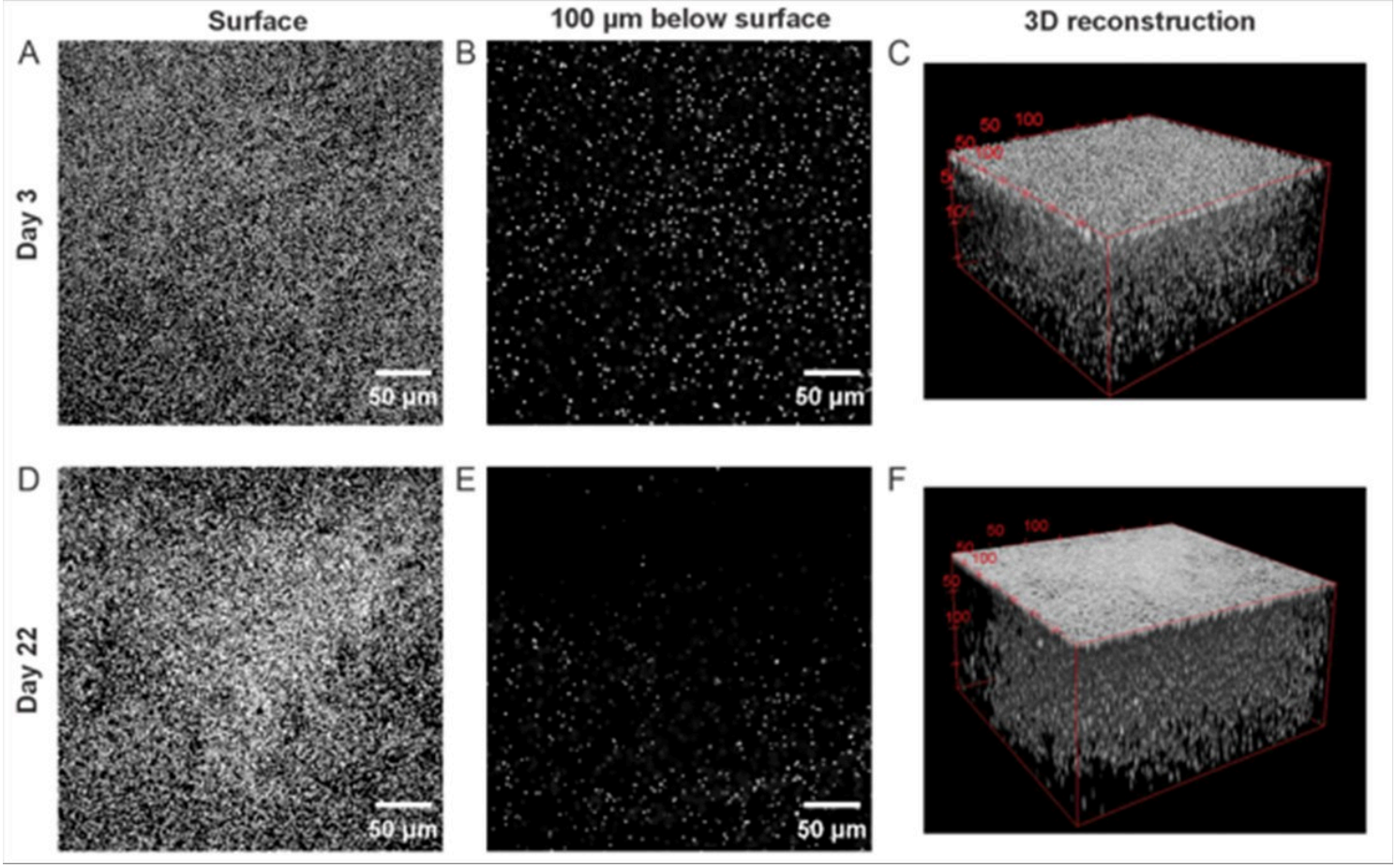

Figure 3

Microscopic visualization of *Synechocystis* cellls immobilised in hydrogel films. A.-F. Laser scanning confocal microscopic images showing chlorophyll autofluorescence of embedded cells from the surface and approximately 100 µm below the surface of the hydrogel after 3 days (A-B) and 22 days (D-E) of cultivation. 3D images reconstructed from single confocal microscope images of the hydrogel on (C) Day 0 and (F) Day 22.

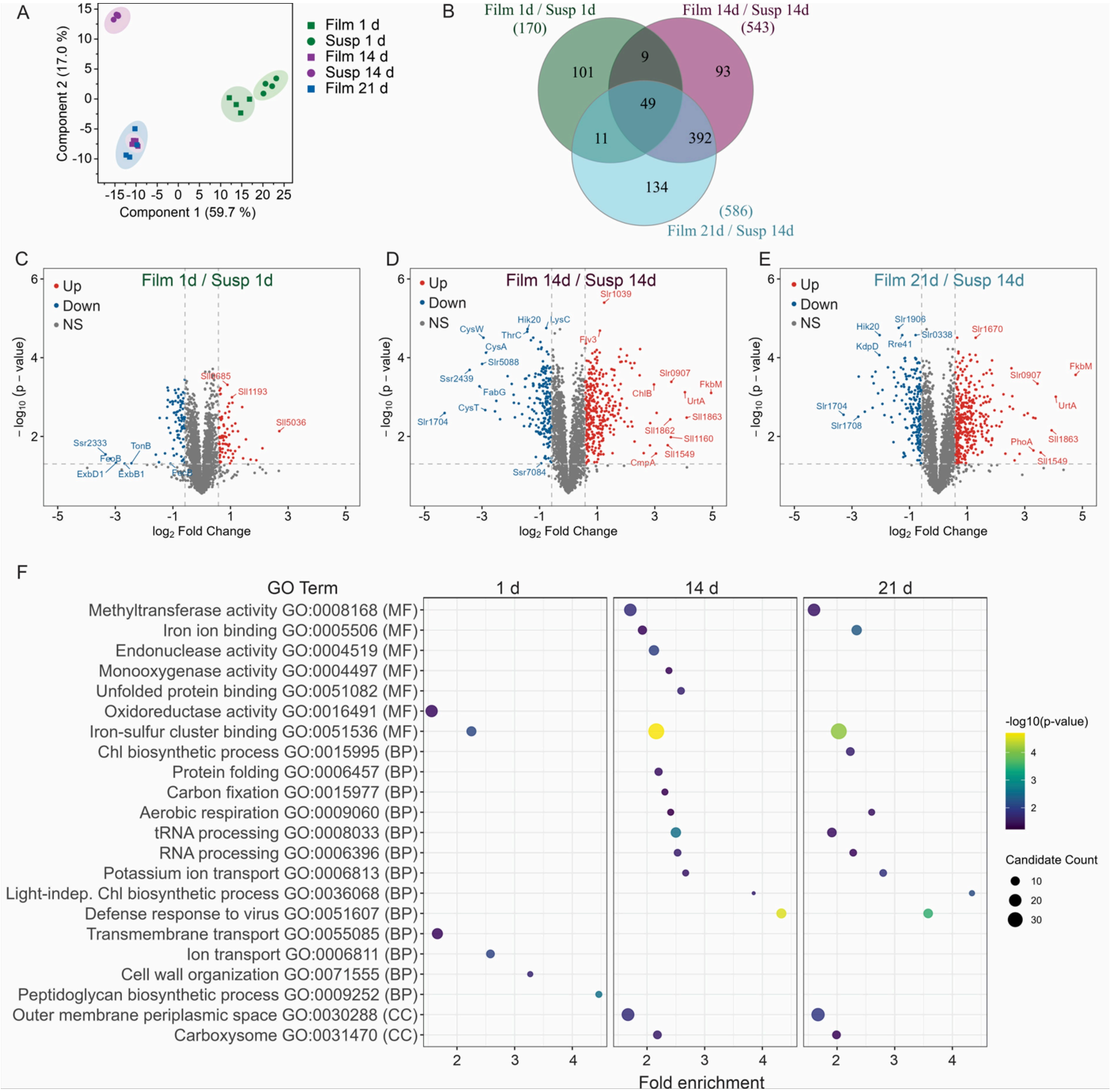

Figure 4

Differentially expressed proteins in *Synechocystis* after 1, 14 and 21 days of immobilization in hydrogel films. A. Principal component analysis (PCA) of proteins, each point represents a sample, with the colour indicating sample collection time and a square represents cells immobilized in alginate hydrogel films (Films) and a circle represents suspension cultures (Susp). Proteomics analysis consisted of four biological replicates in each time point. B. Venn diagram showing the differentially expressed proteins that are commonly or uniquely detected in each comparison. Volcano plots depicting the expression profile of differentially expressed proteins after 1d (C), 14d (D) and 21d (E) of immobilization in

comparison to suspension cultures. F. Gene ontology (GO) enrichment analysis of differentially expressed proteins. Bubble size indicates the number of enriched proteins. Colour saturation represents the significance level. GO terms are divided into three categories: molecular function (MF), cellular component (CC) and biological process (BP). Indep. = independent.

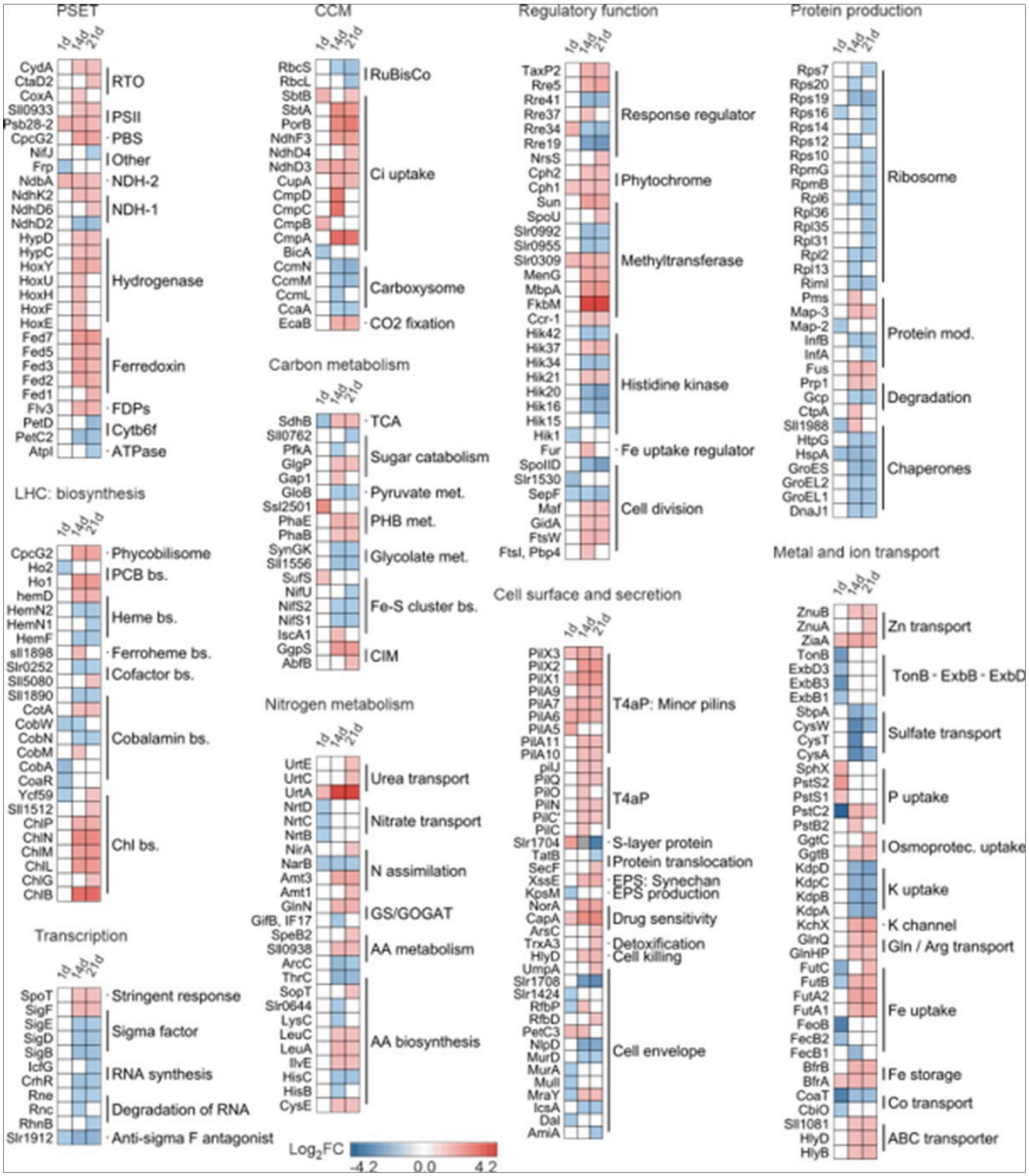

Figure 5

Heatmaps representing significant differential protein expression in immobilized cells compared with suspension cells after 1 d, 14 d and 21 days of immobilization within hydrogel films. Red shades indicate enhanced protein abundance, while blue shades indicate decreased protein abundance. Colour-coded changes correspond to proteins meeting the significance criteria of $p \leq 0.05$ and $\log_2FC \geq 0.58$ or ≤ -0.58, while white indicates non-significant changes.

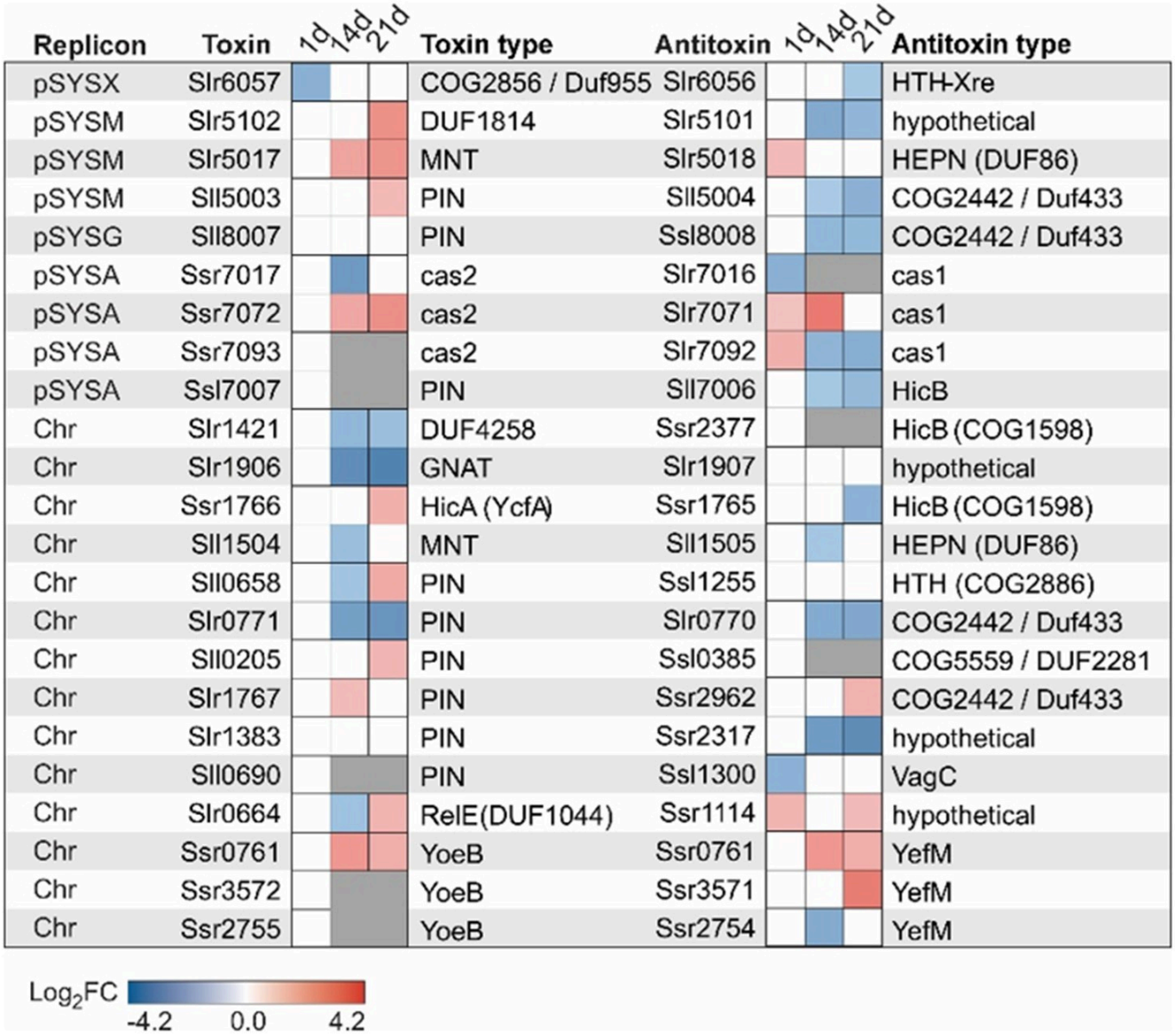

Figure 6

Type II toxin-antitoxin (TA) systems of *Synechocystis* showing significantly different abundance in immobilized vs suspension cultures at least in one timepoint. One toxin and antitoxin pair are shown in a row together with the replicon site. Predicted toxin types are defined according to (105). Red shades indicate enhanced protein abundance while blue is used for decreased protein abundance. Colour indicate significant changes with cut-off threshold $p \leq 0.05$ and $\log_2FC \geq 0.58$ or ≤ -0.58. Grey colour indicates that protein was not detected.

Supplementary Files

This is a list of supplementary files associated with this preprint. Click to download.

- Supplementaryfigures.docx
- Supplementarytables.xlsx